JMEPEG (2010) 19:135–141
DOI: 10.1007/s11665-009-9430-x

1059-9495/$19.00

Investigation of Stainless Steel Corrosion in Ultrahigh-Purity Water and Steam Systems by Surface Analytical Techniques

Xia Dong, Ronald G. Iacocca, Bethany L. Bustard, and Craig A. J. Kemp

(Submitted August 13, 2008; in revised form March 6, 2009)

Stainless steel pipes with different degrees of rouging and a Teflon®-coated rupture disc with severe corrosion were thoroughly investigated by combining multiple surface analytical techniques. The surface roughness and iron oxide layer thickness increase with increasing rouge severity, and the chromium oxide layer coexists with the iron oxide layer in samples with various degrees of rouging. Unlike the rouging observed for stainless steel pipes, the fast degradation of the rupture disc was caused by a crevice corrosion environment created by perforations in the protective Teflon coating. This failure analysis clearly shows the highly corrosive nature of ultrapure water used in the manufacture of pharmaceutical products, and demonstrates some of the unexpected corrosion mechanisms that can be encountered in these environments.

Keywords corrosion, pharmaceutical, rouge, stainless steel, surface analysis

1. Introduction

Stainless steel is often chosen as the material of construction for processing equipment used in the chemical and pharmaceutical industries because of its inherent corrosion resistance and the ease of use. Under some environments, stainless steel is not inert and degradation of stainless steel may occur through different mechanisms. In ultraclean water and steam systems, specifically, those required for the production of pharmaceutical products, the degradation of stainless steel often leads to the generation of particles—a highly undesirable phenomenon.

The process, known as rouging, begins with the formation of a thin yellow surface film, that if allowed to grow, will proceed (in color progression) to black, at which time, if the oxide layer is thick enough, the scale will spall and generate particles downstream.

Information in the pharmaceutical industry has focused on the general description of rouge (Ref 1). Various scenarios have been put forth to describe the formation of rouge and to characterize it. Additional work has been published to describe the various stages/types/of rouge (Ref 2). Tverburg has described three classes of rouge. Class 1 appears as an orange/magenta film comprising particles that are electrostatically attached to the surface. The particles are removed by ultrasonic cleaning. The following reactions have been proposed:

$$2Fe^0 + 4H_2O \rightarrow 2FeO(OH) + 3H_2 \uparrow \quad \text{(Eq 1)}$$

producing an orange discoloration, or

$$2FeO(OH) + 2H_2O \rightarrow Fe_2O_3 + 3H_2 \uparrow \quad \text{(Eq 2)}$$

or

$$2Fe^0 + 3H_2O \rightarrow Fe_2O_3 + 3H_2 \uparrow \quad \text{(Eq 3)}$$

producing a magenta discoloration.

Class 2 rouge typically occurs in the presence of chlorides. The scale that forms must be removed by mechanical or chemical means. The result is a red discoloration and the following mechanisms have been proposed:

$$\begin{aligned} &Cr_2O_3 + 10Cl^- + 2H_2O \rightarrow 2CrCl_3 + 4HClO \\ &2Fe^0 + 3ClO^- \rightarrow Fe_2O_3 + 3Cl^- \end{aligned} \quad \text{(Eq 4)}$$

Note that with Class 2 rouge, both chromium and iron are active species in the degradation reaction.

For Class 3 rouging, the species that forms is not Fe_2O_3 (hematite) but rather Fe_3O_4 (magnetite). Because of this, the scale is blue-black in color and cannot be removed by simple cleaning. The mechanism follows the expected reactions for magnetite:

$$\begin{aligned} &Fe^0 + H_2O \rightarrow FeO + H_2\,(g) \\ &2FeO + H_2O \rightarrow Fe_2O_3 + H_2\,(g) \\ &FeO + Fe_2O_3 \rightarrow Fe_3O_4 \end{aligned} \quad \text{(Eq 5)}$$

Because nearly all of the above reactions include the oxidation of iron, the primary mechanism used to control the formation of rouge in clean water systems is to introduce chemical agents that reduce iron at the interior surface of the pipe, thereby preventing the formation of any iron oxide (Ref 1). According

Xia Dong, Ronald G. Iacocca, Bethany L. Bustard, and **Craig A.J. Kemp**, Eli Lilly and Company, DC 3811, Indianapolis, IN 46285. Contact e-mail: dong_xia@lilly.com.

to Banes, passivation imparts several benefits through (Ref 3): (1) enhanced corrosion resistance, (2) a contaminant-free environment, (3) longevity of the system, and (4) system purity. This increased corrosion resistance, in theory, is derived by the formation of chromium oxide, which is more adherent than iron oxide. It should form a passive layer between the interior of the stainless steel pipe and the water/steam being transported. Regardless of the theory behind passivation, practically speaking, rouge can quickly form even after such treatments, particularly in the presence of superheated steam. More in-depth analyses are required to understand the formation of this discoloration.

For stainless steel, rouging is a commonly observed long-term phenomenon, but it can also be degraded at a speed much faster than expected under certain environments in pharmaceutical manufacturing. Insidious corrosion, or corrosion that occurs in localized environments rather than generalized corrosion, can be extremely destructive because of the difficulty in detecting the corrosion event. Pitting and crevice corrosion are examples of this scenario. An example will be provided on the corrosion of Teflon-coated rupture discs used in stainless steel tanks to prevent the generation of excessive pressure in containment vessels. The Teflon coating was applied to impart corrosion resistance over that of unprotected 316L stainless steel; however, inadvertently, a more aggressive corrosion environment was created.

In this article, optical imaging, SEM (secondary electron microscopy)/EDS (energy dispersive x-ray spectroscopy), AES (Auger electron spectroscopy), and TOF-SIMS (time of flight-secondary ion mass spectrometry) were used to investigate both rouge formation, when stainless steel is exposed to water or steam, and the discoloration of rupture discs used in stainless steel tanks. The relationship between the iron oxide layer thickness, the surface roughness, and the extent of rouge development was studied by SEM and AES.

In the case of the stainless steel rupture disc, the application of a Teflon coating caused the degradation to occur at specific locations on the device. Using the same tools mentioned above, data are given on both the loss of integrity of the Teflon and as on the degradation of the stainless steel substrate.

2. Experimental

Three stainless steel pipes, with different degrees of rouging, were cut into small pieces for optical imaging and AES analysis. Every effort was made to minimize the possibility of surface contamination during the sample preparation process. The discolored rupture disc, which was made from 316L stainless steel with a Teflon membrane coating, was removed from a 1000 gallon 316 stainless steel tank used as a water container for a cleaning in place (CIP) system.

The SEM and ESEM images and EDS spectra were obtained using a Philips XL30 ESEM with a PGT IMIX EDS system. Images were captured at varying magnifications using the Everhardt-Thornley secondary electron detector for the stainless steel pipes and using a gaseous secondary electron detector for the rupture disc.

All TOF-SIMS spectra and images were collected using a Physical Electronics (Chanhassen, MN) TRIFT-III instrument, equipped with a 15 kV Ga^+-focused liquid metal ion gun. The primary ion beam (DC) current was approximately 700 pA. The high mass resolution spectra were collected using a bunched primary ion beam while an unbunched beam was used to provide high spatial resolution images. Charge compensation was achieved with an auxiliary low-energy electron flood gun that was engaged between primary ion pulses.

The depth profiles of the stainless steel pipes with various extents of rouge were collected with a Physical Electronics 690 Scanning Auger Microscope, using a 10 kV, 10 nA electron beam. The sputtering rates were determined based on a SiO_x standard. The etch-depth defining oxide/substrate interface was identified by locating the point at which the oxygen signal decreased to its half-maximum value.

Three stainless steel pipes with various histories were first examined using an optical microscope. Pipe 1 was mechanically polished and had never been exposed to water or steam. This pipe was used as a control sample. Pipe 2 was also mechanically polished and had been exposed to 80 °C water for a short time period, although the exact time is unknown. Pipe 3 had been retired after a long period of service in the water system. The exact sample history was not known. The nominal roughnesses of pipes (Ra) are about 10, 14, and 94 microinch for Pipes 1, 2, and 3, respectively.

3. Results and Discussion

3.1 Rouge Investigation

To understand the extent of rouging, SEM micrographs of the three pipe samples were obtained, as shown in Fig. 1. Pipe 1 received no exposure to high-temperature water or steam, Pipe 2 is in the preliminary stages of rouging, exhibiting a yellow-colored oxide scale, and Pipe 3 is at a more advanced stage of rouge, exhibiting a red-colored oxide scale. In SEM micrographs, the control sample surface (Fig. 1a) exhibits the original mechanical polishing features that would be expected in a mechanically polished material. The micrograph of Pipe 2 (Fig. 1b) shows the same polishing features, though to a more severe extent. This increased severity is not caused by exposure to a corrosive environment but rather is an artifact of mechanical polishing. Because these features are readily visible, this material is in the early stages of oxidation. The Pipe 3 surface contains ‘‘island’’ features, as shown in Fig. 1c, and appears rougher than the other two pipes, indicating more severe degradation occurring on this sample.

As discussed earlier, the rouging phenomenon involves the formation of iron oxide, regardless of the mechanisms behind it. Figure 2 compares the AES depth profiles of certain elements obtained from the three pipes. The control sample (Pipe 1) has the thinnest oxide layer at approximately 25 nm (Fig. 2a). Depth profiles taken from Pipe 2 in an area where the oxide layer appears yellow in color has been oxidized to a depth of approximately 200 nm (Fig. 2b). In comparison, depth profiles obtained from Pipe 3 (Fig. 2c), where the oxide layer was red in color, had an oxide layer varying from 600 to 1200 nm. The SEM picture of Pipe 3 shows island-like structures, and the surface appearance is not uniform. The variable thickness and location of the oxide is most likely caused by localized differences in the stainless steel surface. The spectra in Fig. 2 also reveal that there is no preferential oxidation occurring in the sample, as evidenced by the profiles obtained for chromium oxide. (Note that the thicknesses of the

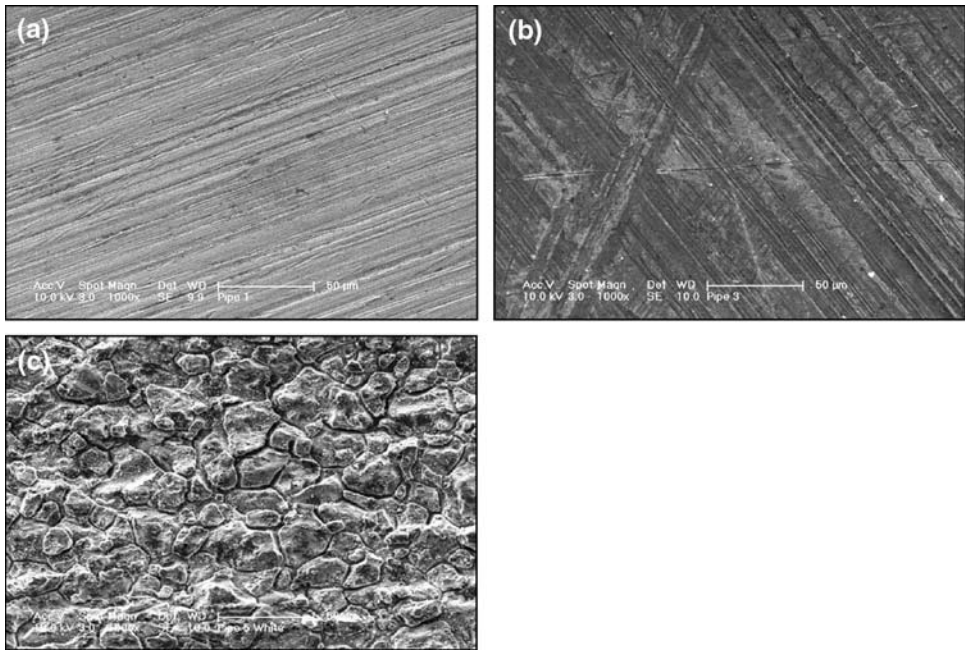

Fig. 1 Scanning electron micrograph of stainless steel pipes with various rouge extent. (a) Pipe 1—mechanical polished pipe used as a control. (b) Pipe 2—mechanical polished pipe exposed to 80 °C H_2O. (c) Pipe 3—pipe after long service

oxide layer were calculated based on the sputtering rate obtained from a silicon oxide standard; therefore, the absolute measurement may not be accurate. However, the relative comparison between different samples is still valid.)

It has been suggested in previous research in the rouging process that chromium oxide may preferentially form at the metal/water (or steam) interface because of its thermodynamic stability and tenacity as compared to various oxides of iron; however, chromium oxide depletion is not observed in the current work. Such observations may have been detected on samples that have undergone a passivation treatment, where iron is intentionally removed from the interface, allowing chromium oxide to form preferentially.

3.2 Failure Analysis of Rupture Disc

Although rouge is considered to be a uniform corrosion/oxidation phenomenon, the following example will illustrate how the corrosion mechanism can become an insidious phenomenon occurring in a very localized fashion.

Figure 3 shows the optical images of a corroded rupture disc (coated with Teflon) that was installed in a stainless steel tank used as a water container. Discoloration occurred on multiple discs shortly after installation. In service, these discs were exposed to clean steam and water. Note the severity and localized nature of the degradation. Cracking and holes caused by corrosion were confined to the rim area of the disc, where the Teflon gaskets are located. Figure 4(a) to (c) shows the ESEM micrographs of the corroded surface, revealing the granular surface structure that is encountered with the corrosion of ferrous alloys (Fig. 4a), the detail on the cracking of the surface that takes place during corrosion, often referred to as "mud cracking" (Fig. 4b), and an area containing pits (Fig. 4c). Figure 4d shows the same corroded microstructure in close proximity to the Teflon coating, which has lost its integrity as a protective surface.

The elemental composition of the Teflon-coated area and the area experiencing severe corrosion detected by EDS are listed in Tables 1 and 2, respectively. The results show that fluorine is a major element in the Teflon-coated area.

Since the x-ray emission lines from fluorine and iron overlap in the EDS spectrum, it is impossible to adequately map these elements by EDS. TOF-SIMS is a powerful technique that can provide chemical imaging with high spatial resolution, and allows the imaging of molecular species, thereby eliminating the overlap encountered with EDS. Additionally, this technique has been applied to corrosion investigations in the past (Ref 4-7). In particular, the spectra produced from fluorocarbons are quite distinct (Ref 8). Therefore, TOF-SIMS was used to provide compositional mapping of a section of the failed rupture disc.

The positive ion spectra collected from two areas on the rupture disc—one where corrosion had occurred and another where corrosion was not yet evident—are presented in Fig. 5. The spectrum from the corroded area is dominated by *m/z* 56 ($^{56}Fe^+$) and *m/z* 52 ($^{52}Cr^+$) ions from the exposed metal surface. The spectrum from the noncorroded area contains intense ions at *m/z* 12 (C^+), 31 (CF^+), 69 (CF_3^+), 119 ($C_2F_5^+$), 131 ($C_3F_5^+$), and resembles a library spectrum of Teflon (Ref 8). The peak intensities are represented by the secondary ion counts detected from the analytical area.

The high spatial resolution images were collected from several areas on the sample. Ion images are presented for three different areas in Fig. 6. The left column represents the summation of the intensities of the most abundant fluorocarbon ions (see above), and the right column represents the summation of the intensities of *m/z* 52 and 56 (Cr^+ and Fe^+, respectively). The middle row of images was produced from a clear, corrosion-free region. The top and bottom rows were produced from corroded regions.

The fluorocarbon ions from the Teflon coating contribute the majority of the signal in the image collected from the

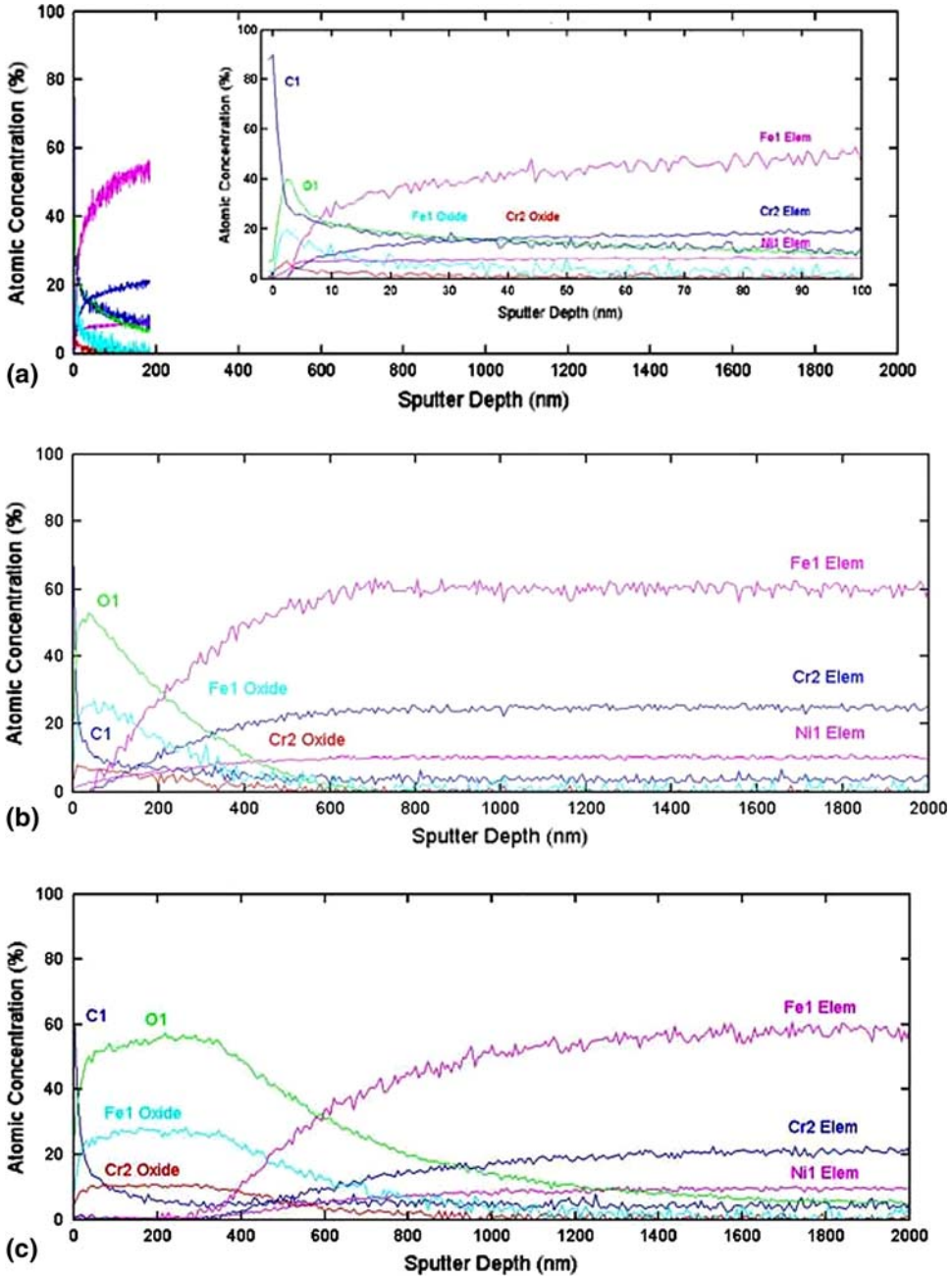

Fig. 2 AES depth profiles of stainless steel pipes with various rouge extent. (a) (top) Mechanically polished pipe used as a control. (b) (middle) Mechanically polished pipe exposed to 80 °C H_2O. (c) (bottom) Pipe after long service

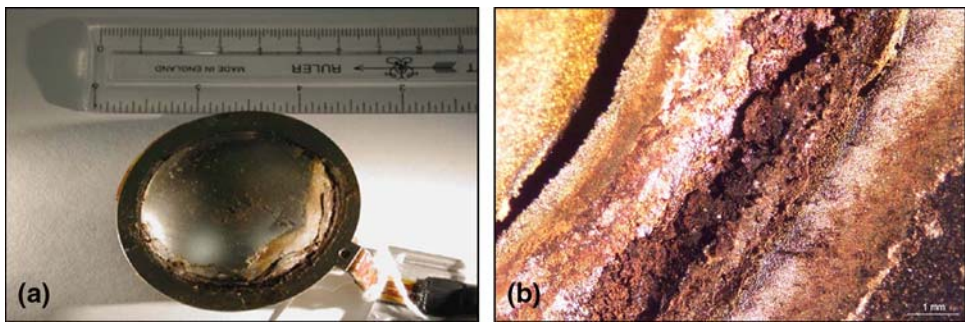

Fig. 3 Optical macroscopic images of corroded rupture disc

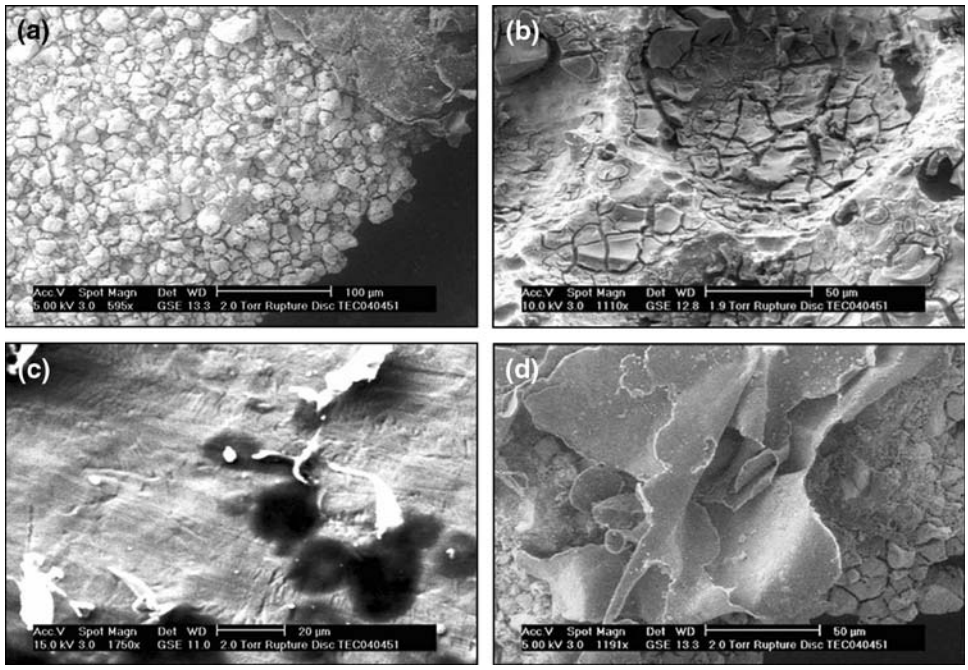

Fig. 4 Scanning electron micrographs of the surface of a rupture disc, showing a breach in the coating and the corrosion that ensued

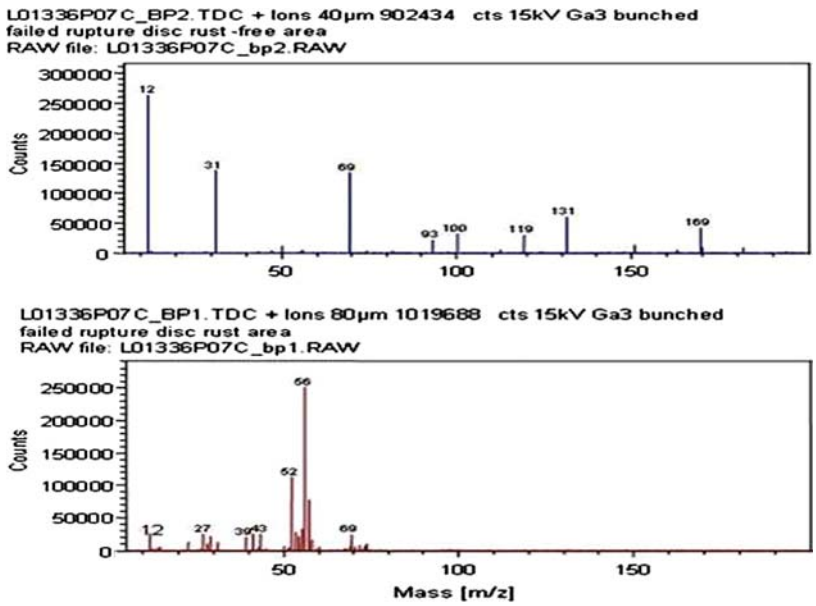

Fig. 5 Positive ion TOF-SIMS spectra taken from two areas on the failed rupture disc. Top: no visible corrosion. Bottom: corroded area

Table 1 Relative elemental composition of intact coating area

Elements	Normal weight %
C	17.96
Ni	0.02
F	23.83
Cr	0.06
Mn	0.00
Fe	0.15
O	57.98

Table 2 Relative elemental composition of corroded area

Elements	Normal weight %
C	0.99
Ni	5.85
F	20.99
Si	0.15
S	0.25
Cr	7.38
Mn	1.05
Fe	35.78

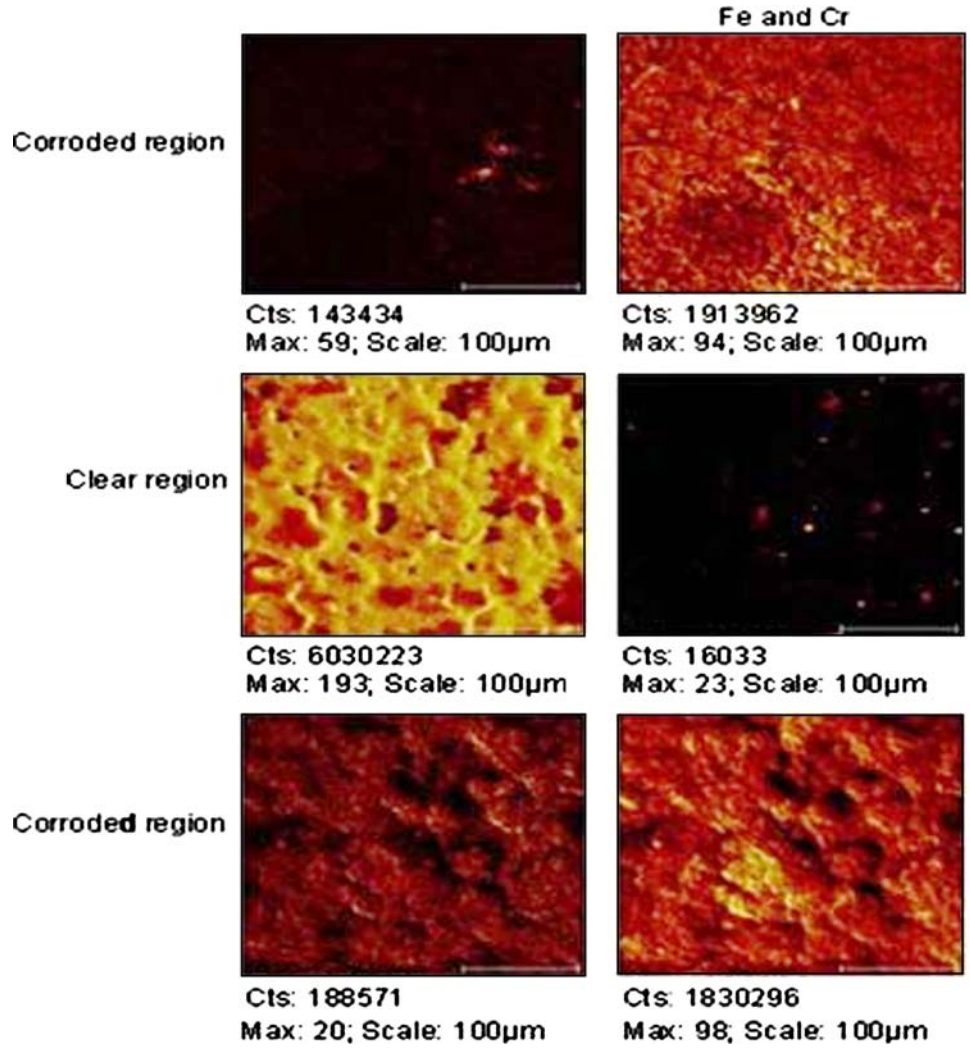

Fig. 6 TOF-SIMS ion images from two areas in the corroded region of the rupture disc (top and bottom rows) and the noncorroded region (middle row). The images in the left column of images are derived from signals from *m/z* 31, 69, 119, 131, and 169 (fluorocarbon-related peaks), and images in the right column are derived from *m/z* 52 and 56 (Cr^+ and Fe^+, respectively)

corrosion-free region while spots enriched with Fe/Cr were also detected. The top row of images in Fig. 6 reveals the presence of a residual ragged patch of fluorocarbon on the corroded metal; whereas the bottom row indicates that the area from which those maps were produced contains no distinct fluorocarbon "islands," and a low-level signal in the fluorocarbon map matches the appearance of Fe/Cr maps. The TOF-SIMS results suggest that the Teflon layer is relatively intact in the corrosion- free area; however, its integrity was compromised in the corroded area. These results are consistent with ESEM observation.

The results obtained from the optical imaging, SEM/EDS, and TOF-SIMS suggest that the loss of integrity of the Teflon-coated layer has allowed water or other chemicals used in the cleaning process to concentrate at the Teflon/metal interface, creating an extremely aggressive environment, combining the mechanisms of crevice corrosion and rouging. Because of the physical location of the corrosion, it is also believed that the Teflon gasket used in the sanitary fitting accelerated the corrosion. Therefore, it is proposed that the Teflon coating, combined with the existence of the Teflon gasket, has created an insidious corrosion mechanism that is causing in situ failure of the rupture discs.

In addition to removing the Teflon coating to eliminate the crevice corrosion environment, one could substitute nickel-base alloys as such materials exhibit a greater resistance to corrosion (Ref 9). However, because the vast majority of this system is stainless steel, such a materials substitution might well create a galvanic couple.

4. Conclusions

It is demonstrated that surface morphology changes with rouging extent, and oxide layer thickness increases with rouging formation. In studying the rouging of stainless steel pipes used to transport clean steam and water for pharmaceutical processing, by monitoring oxide growth instead of reacting to particles detected in water for injection, it should be possible to develop a preventative maintenance schedule to eliminate the impact of rouge on the water quality.

The failure analysis of a Teflon-coated rupture disc demonstrated how a protective coating can actually create a more aggressive corrosion environment. By combining the imaging capabilities of TOF-SIMS and SEM, it was shown that perforations in the Teflon coating, combined with unoptimized placement of a gasket, was responsible for the destruction of the device. Rouging was actually turned into a localized, insidious corrosion event.

References

1. T. Self, P. Olsen, and P. Banes, Investigating the Rouging of Stainless Steel USP Water Systems, *Microcontamination*, 1993, **11**(5), p 44–55
2. J.C. Tverberg, Rouging of Stainless Steel in Pharmaceutical Systems, *AIChE Spring National Meeting*, 10-14 April 2005 (Atlanta, GA), American Institute of Chemical Engineers, New York, 2005, p 10016-5991
3. P.H. Banes, Fundamentals of Passivation, *AIChE Spring National Meeting*, 10-14 April 2005 (Atlanta, GA), American Institute of Chemical Engineers, New York, 2005
4. T. Numata, H. Nanao, S. Mori, and S. Miyake, Chemical Analysis of Wear Tracks on Magnetic Disks by TOF-SIMS, *Tribol. Int.*, 2003, **36**, p 305–309
5. J.T. Francis, N.S. McIntyre, R.D. Davidson, S. Ramamurthy, A.M. Brennenstühl, A. McBride, and A. Roberts, Mechanisms of Pitting Corrosion in Alloy N04400 as Revealed by Imaging XPS, TOF-SIMS and Low-Voltage SEM, *Surf. Interface Anal.*, 2002, **33**, p 29–34
6. M.F. Fitzpatrick, J.F. Watts, and J.S.G. Ling, Failure Mechanism of Adhesively Bonded Hot Dipped Galvanised Steel: A TOF-SIMS and XPS study, *Polym. Mater. Sci. Eng.*, 1999, **81**, p 417–418
7. A.C. Lloyd, J.J. Noel, S. Mclntyre, and D.W. Shoesmith, Cr, Mo and W Alloying Additions in Ni and Their Effect on Passivity, *Electrochim. Acta*, 2004, **49**, p 3015–3027
8. J.G. Newman, B.A. Carlson, R.S. Michael, J.F. Moulder, and T.A. Hohlt, *Static SIMS Handbook of Polymer Analysis*, Perkin-Elmer Corporation, Eden Prairie, MN, 1991
9. W.Z. Friend, *Corrosion of Nickel and Nickel-Base Alloys*, Wiley, New York, 1980, p 459